

Supporting Information

3D protein structure determination using pseudocontact shifts of backbone amide protons generated by double-histidine Co²⁺-binding motifs at multiple sites

Alireza Bahramzadeh, Thomas Huber, and Gottfried Otting**

Research School of Chemistry, Australian National University, Canberra, ACT 2601
(Australia)

Table S1. $\Delta\chi$ tensor parameters of ERp29-C fitted to the structure 2M66¹ using the PCSs measured with dHis-Co²⁺ motifs.^a

		Mu1	Mu2	Mu3	Mu4
$\Delta\chi_{ax}$ ^b		-2.3	-1.8	-3.1	3.1
$\Delta\chi_{rh}$ ^b		-0.7	-1.1	-1.0	1.0
Metal coordinates ^c	x	4.957	-3.581	13.597	23.499
	y	17.411	8.383	16.046	13.816
	z	11.492	-10.399	14.731	-4.848
Euler angles (degrees) ^{c,d}	α	155	77	158	75
	β	122	133	96	156
	γ	134	55	24	128
SD (ppm ²) ^e		0.031	0.012	0.039	0.043
RMSD (ppm) ^f		0.020	0.013	0.021	0.027
<i>Q</i> -factor ^g		0.24	0.21	0.23	0.27

^a The program Numbat² was used to fit the $\Delta\chi$ tensors. The fit used all residues of all 11 conformers of 2M66 to determine the $\Delta\chi$ tensor, which yielded the lowest squared deviation between back-calculated and experimental PCSs. The fits were performed without restricting the position of the metal ion. The experimental PCSs are reported in Table S2.

^b In units of 10⁻³² m³.

^c Relative to the coordinates reported in the PDB file 2M66.

^d Expressed in the 'ZYZ' convention.

^e Sum of the square deviation of back-calculated and experimental PCSs.

^f Root mean square deviation of back-calculated and experimental PCSs.

^g Calculated as $\text{Sqrt}[\sum(\text{PCS}_{\text{exp}} - \text{PCS}_{\text{calc}})^2 / \sum(\text{PCS}_{\text{exp}})^2]$, where PCS_{exp} and PCS_{calc} are the experimental and back-calculated PCSs, respectively.

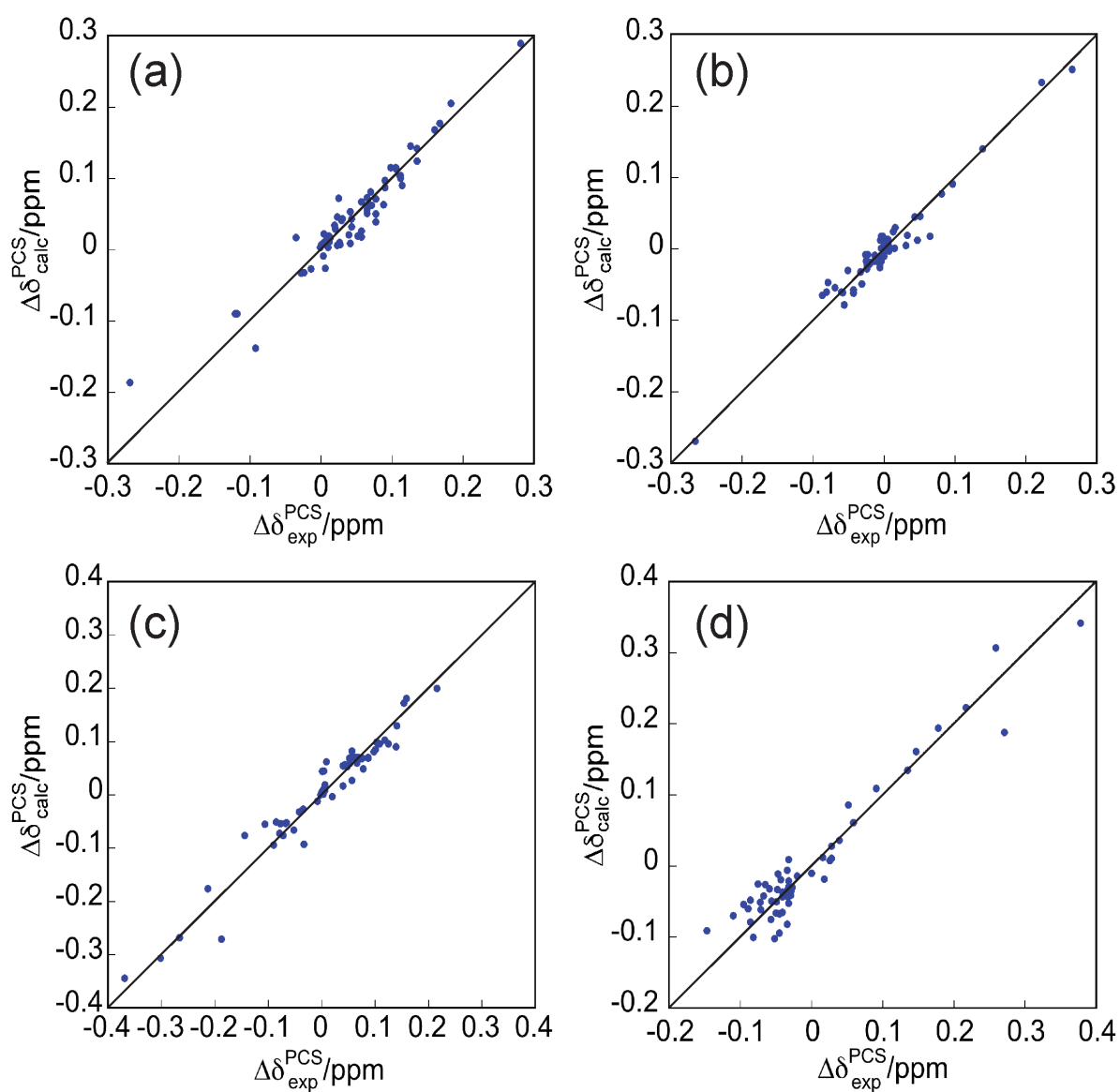


Figure S1. Correlation between back-calculated and experimental PCSs for the four different mutants of ERp29-C (Mu1 – Mu4), each of which contains a dHis-Co²⁺ motif at a different site. The $\Delta\chi$ tensors of Table S1 were used for the back-calculation of the PCSs.

Table S2. Experimental PCSs of the backbone amide protons of ERp29-C with a dHis-Co²⁺ motif at four different sites.^a

Total number of PCSs	73	69	85	58
Residue	PCSs of Mu1	PCSs of Mu2	PCSs of Mu3	PCSs of Mu4
G156			0.001	
C157			0.009	
L158		-0.087	0.052	
A160		-0.031		
Y161		-0.043	0.125	
D162		-0.056	0.020	
A163		-0.058	-0.033	-0.032
L164		-0.079		
A165		-0.06	-0.090	
G166		-0.081	-0.266	-0.034
Q167		-0.033		
F168		-0.006	-0.369	0.026
I169			-0.213	0.002
E170			-0.302	0.018
A171		0.007	-0.188	0
S172	0.281	0.004	0.004	-0.043
S173	0.183	0.006		-0.107
R174	0.090	0.031		-0.046
E175	0.077	0.003		-0.050
A176	0.112	0.003		
R177		0.015		
Q178	0.114	0.004		0.059
A179		0.002		
I180		-0.002		
L181	0.105	-0.013		
K182	-0.028	-0.001		
Q183		0		
G184	-0.024	-0.008		0.217
Q185	-0.001	-0.009		0.378
D186	-0.118	-0.006		0.259
G187	-0.121	-0.01		0.178
L188	0.003	-0.01	0.154	
S189	-0.014	-0.009	0.139	0.147
G190	0.006	-0.01	0.216	0.091
V191	0.057	-0.011	0.159	0.034
K192	0.088	-0.024	0.141	0.039
E193	0.043	-0.012	0.067	0.028
T194	0.043	-0.013	0.044	0.016

D195	0.071	-0.020	0.069	0.028
K196	0.067	-0.020	0.062	
K197	0.057	-0.025	0.048	-0.047
W198	0.090	-0.024	0.053	-0.075
A199	0.135	-0.024	0.057	-0.109
S200	0.111	-0.008	0.076	-0.020
Q201		-0.004	0.040	-0.045
Y202	0.160	-0.051	0.064	
L203	0.167	-0.022	0.109	-0.059
K204		-0.023	0.087	
I205	0.135	-0.026	0.053	
M206		-0.013	0.098	
G207	0.126	0.007	0.103	
K208	0.112	-0.005	0.087	
I209	0.106		0.075	
L210	0.098		0.118	
D211	0.065	0.047	0.101	
Q212	0.065	0.065	0.066	
G213	0.065	-0.004	0.078	
E214	0.052	-0.002	0.057	
D215	0.041		0.040	0.013
F216	0.057	0.043	0.006	
A218	0.023		0.001	-0.052
S219	0.027		0.003	-0.147
E220	0.039		0.005	
L221	0.013		0.001	-0.05
A222	0.010		-0.002	-0.11
R223	0.026		0	-0.057
I224	0.016		0	-0.034
S225	0.008		-0.001	-0.089
K226	0.008		0	-0.056
L227	0.007		0.001	-0.095
I228	0.012	0.265	0	-0.086
E229	0	0.222	0	-0.041
N230	0.002	0.139	0.003	-0.028
K231	0.001	0.097	0	-0.032
M232	0.004	0.081	0	-0.048
S233	0.012	0.051	0.003	-0.037
E234	0.011	0.033	0.002	-0.027
G235	0.011	0.006	0.001	-0.034
K236	0.011	0.013	0.003	-0.039
K237	0.008	0.016	0.004	-0.033
E238	0.004	0	0.004	-0.067
E239	0.020	-0.004	0.006	-0.032

L240	0.020	-0.002	0.006	-0.008
Q241	0.020	-0.006	0.002	0.019
R242	0.029	-0.043	0.005	
S243	0.041	-0.069	0.004	
L244	0.030		0.001	
N245	0.023		0.003	
I246	0.070		0.001	-0.041
L247	0.025	-0.266	0	
T248	0.019		-0.008	
A249	0.077		-0.034	
F250	0.077		-0.038	-0.045
R251			-0.042	
K252	-0.092		-0.068	-0.049
K253			-0.144	
G254	-0.269		-0.106	-0.072
A255			-0.085	-0.029
E256			-0.079	
K257			-0.072	
E258			-0.066	
E259			-0.077	-0.032
L260			-0.052	

^a PCSs were measured in ppm by subtracting the chemical shift of samples with Co²⁺ from samples with Zn²⁺ observed in [¹⁵N,¹H]-HSQC spectra of uniformly ¹⁵N/¹³C-labeled samples at 25 °C in 20 mM MES buffer, pH 6.5, containing 50 mM NaCl buffer.

Table S3. $\Delta\chi$ tensor parameters and cobalt ion coordinates relative to the first conformer of 2M66 and the individual conformers of the Top10 ensemble.^a

Mutant	2M66	top1	top2	top3	top4	top5	top6	top7	top8	top9	top10	
Mu1												
$\Delta\chi_{ax}^b$	-2.63	-2.79	-2.52	-2.66	-2.70	-2.61	-2.81	-2.70	-3.02	-3.16	-3.05	
$\Delta\chi_{rh}^b$	-0.38	-0.34	-0.22	-0.54	-0.51	-0.57	-0.35	-0.62	-0.77	-0.77	-0.68	
Metal coordinates	x	5.80	4.58	4.17	6.62	4.01	4.23	3.63	3.75	3.94	4.30	4.62
	y	15.41	16.78	17.62	16.86	16.46	17.79	17.20	17.16	16.74	16.68	17.09
	z	14.05	13.39	13.14	13.49	13.55	13.04	13.18	12.81	13.30	13.58	13.47
Euler angles (degrees)	α	165	163	162	159	159	148	162	157	157	159	158
	β	112	115	116	108	115	118	117	120	119	116	116
	γ	145	150	140	155	135	146	149	143	149	156	154
SD	0.05	0.02	0.04	0.04	0.03	0.07	0.03	0.04	0.04	0.03	0.04	
Q -factor ^c	0.32	0.18	0.28	0.26	0.25	0.35	0.23	0.28	0.29	0.25	0.27	
Mu2												
$\Delta\chi_{ax}^b$	-2.43	-2.20	-2.66	-2.58	-2.29	-2.40	-2.61	-2.45	-2.52	-2.37	-2.32	
$\Delta\chi_{rh}^b$	-1.54	-1.21	-1.54	-1.15	-1.08	-1.45	-1.68	-1.57	-1.54	-1.08	-1.45	
Metal coordinates	x	-2.66	-1.38	-1.07	-0.55	-0.91	-4.28	-1.78	-2.06	-1.60	0.35	-3.06
	y	19.92	19.65	20.21	20.26	18.99	18.96	20.48	19.62	19.57	20.89	19.60
	z	-11.84	-13.01	-14.34	-14.39	-15.18	-10.69	-12.66	-12.15	-12.97	-15.06	-10.91
Euler angles (degrees)	α	66	67	60	59	52	80	62	63	60	58	75
	β	130	142	142	141	152	130	138	136	136	151	135
	γ	51	50	45	39	38	62	54	49	45	54	65
SD	0.01	0.03	0.03	0.02	0.03	0.02	0.04	0.03	0.02	0.06	0.04	
Q -factor ^c	0.22	0.29	0.31	0.25	0.32	0.27	0.38	0.30	0.24	0.45	0.35	
Mu3												
$\Delta\chi_{ax}^b$	-3.94	-4.10	-3.51	-2.64	-3.87	-3.64	-3.95	-3.23	-3.67	-3.39	-3.97	
$\Delta\chi_{rh}^b$	-2.08	-1.78	-1.22	-0.77	-1.70	-1.43	-1.64	-1.17	-1.44	-1.34	-1.81	
Metal coordinates	x	17.78	14.78	14.22	13.74	14.47	14.17	14.49	13.78	14.02	14.35	15.01
	y	16.63	15.96	15.96	16.34	15.43	16.08	15.77	15.75	16.20	16.11	15.93
	z	14.35	14.75	14.96	14.02	14.84	14.64	14.73	14.80	14.67	14.52	14.57
Euler angles (degrees)	α	154	150	152	157	153	151	152	154	154	155	150
	β	84	94	98	96	92	95	93	99	97	92	90
	γ	44	28	28	22	26	27	27	24	27	28	32
SD	0.11	0.03	0.07	0.05	0.06	0.05	0.04	0.07	0.03	0.06	0.06	
Q -factor ^c	0.37	0.19	0.29	0.25	0.27	0.25	0.24	0.30	0.20	0.27	0.29	

Mu4												
$\Delta\chi_{ax}^b$		1.84	2.65	2.26	2.12	2.21	2.17	1.99	2.68	2.30	1.71	2.04
$\Delta\chi_{rh}^b$		1.12	1.39	1.19	1.08	1.20	1.23	1.15	1.48	1.14	0.95	1.18
Metal coordinates	x	20.47	21.00	19.81	20.21	20.79	20.54	20.50	20.28	21.07	20.78	20.47
	y	15.95	16.00	15.90	15.58	16.14	16.06	15.70	16.41	14.94	15.98	16.98
	z	-2.56	-5.00	-4.98	-4.54	-3.75	-3.82	-3.44	-5.45	-4.32	-2.16	-2.80
Euler angles (degrees)	α	92	95	96	91	90	89	88	101	86	80	91
	β	139	145	147	145	141	141	142	144	149	142	134
	γ	145	137	140	142	136	141	137	140	134	134	143
SD		0.07	0.07	0.06	0.06	0.06	0.07	0.10	0.09	0.11	0.06	0.10
<i>Q</i> -factor ^c		0.35	0.35	0.33	0.33	0.31	0.35	0.41	0.40	0.44	0.32	0.42

^a The metal coordinates were determined by modeling the dHis-Co²⁺ motif using a PyParaTools³ module, which finds the metal coordinates with minimal RMSD with regard to the expected carbon-metal distances of the dHis-Co²⁺ motif (Figure 3b). The remaining $\Delta\chi$ tensor parameters were determined using the program Numbat² with the metal position fixed to these coordinates.

^b In units of 10^{-32} m^3 .

^c Calculated as the root-mean-square (RMS) of the differences between experimental and back-calculated PCSs divided by the RMS of the experimental PCSs.

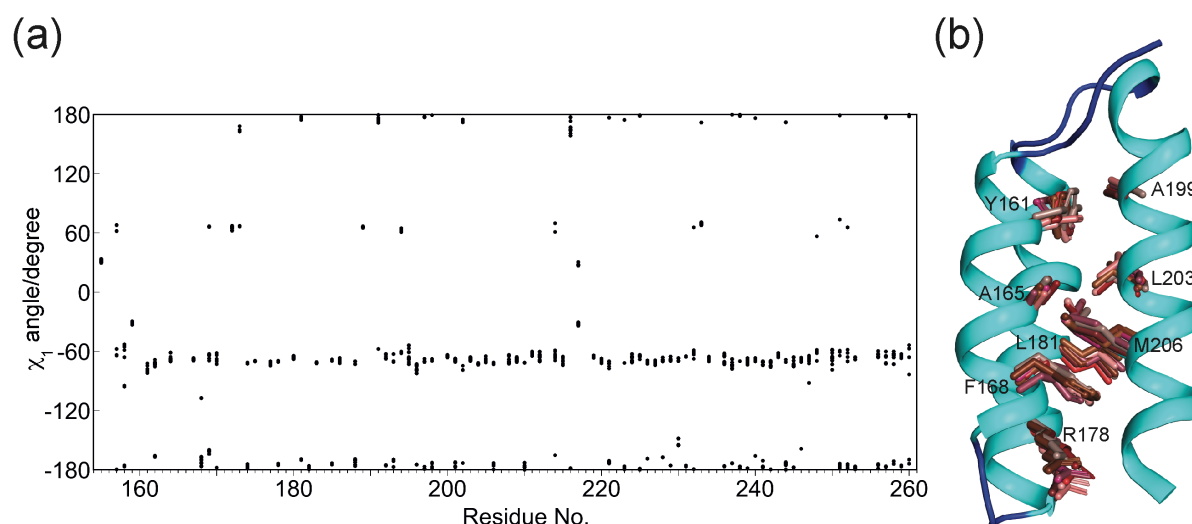


Figure S2. Side chain conformations determined by the GPS-Rosetta calculations. χ_1 angles of all residues in the Top10 conformers. (b) Illustration of precision of side chain conformations of buried residues from helices 5–7 in the Top10 conformers (plotted in shades of red) following C^α atom superimposition of the conformers.

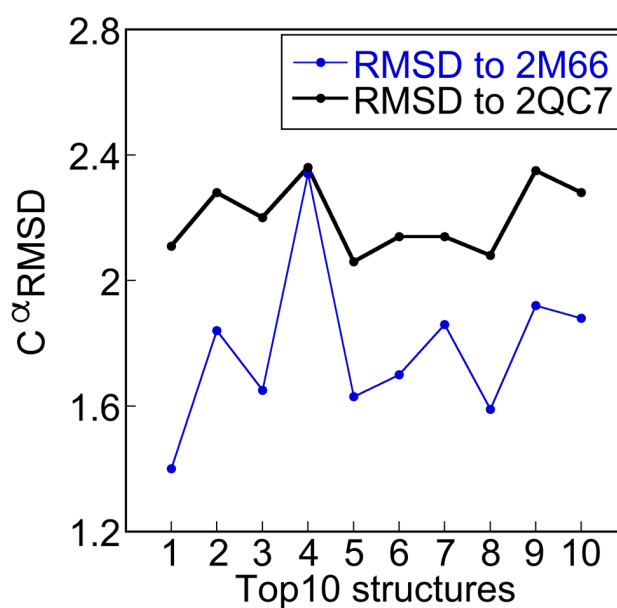


Figure S3. Comparison of the Top10 conformers to the first conformer of the structure 2M66¹ and the crystal structure 2QC7.⁴ The figure reports the C^α RMSD values determined by PyMOL⁵ following superimposition for minimal RMSD. The RMSD values are consistently smaller with respect to 2M66 than 2QC7, with the conformer top1 showing the lowest RMSD to 2M66 (95 residues aligned, comprising residues 156-251 of rat ERp29-C; the rat protein contains one residue less than the human protein (deletion of K230)).

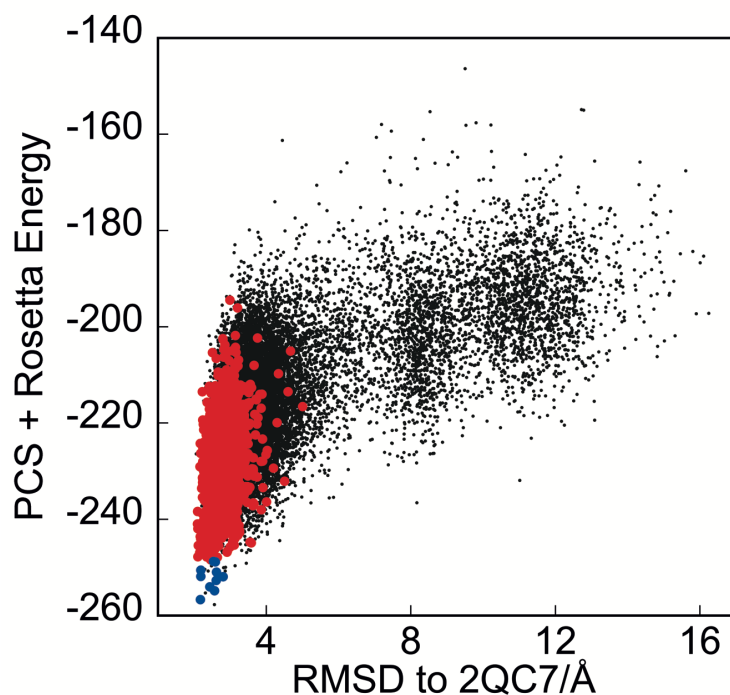


Figure S4. Combined PCS + Rosetta energy scores of the 20,000 GPS-Rosetta structural models (black points) calculated in the present work plotted versus the C α RMSD to the crystal structure of human ERp29 (PDB ID: 2QC7). The alignment included all residues of the C-terminal domain in the crystal structure (155–256). Black points mark the result for all 20,000 structures obtained from GPS-Rosetta. Blue and red points mark the same structures as in Figure 3a, i.e. structures fulfilling the PCS restraints as well as the distance restraints specified in Figure 3b.

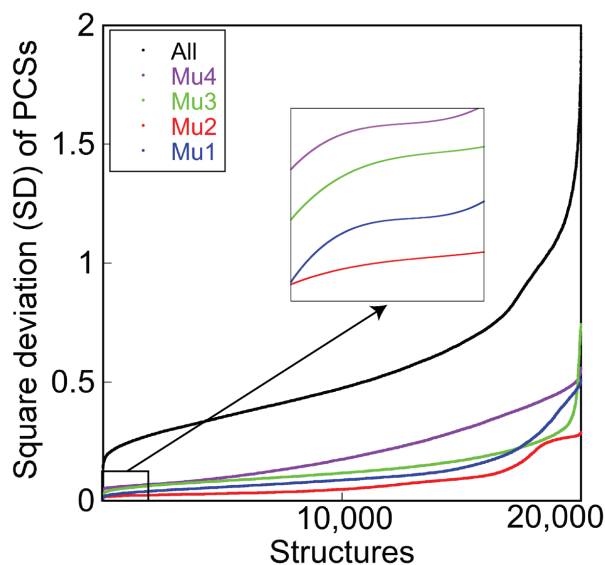


Figure S5. Performance of the PCS data set from each dHis-Co²⁺ motif in the GPS-Rosetta calculations. The GPS-Rosetta models calculated were sorted by their square deviations (SD) between experimental and back-calculated PCSs. The coordinated descent of SD values observed for the four mutants indicates that all four PCS datasets contributed to the overall convergence of the GPS-Rosetta calculations.

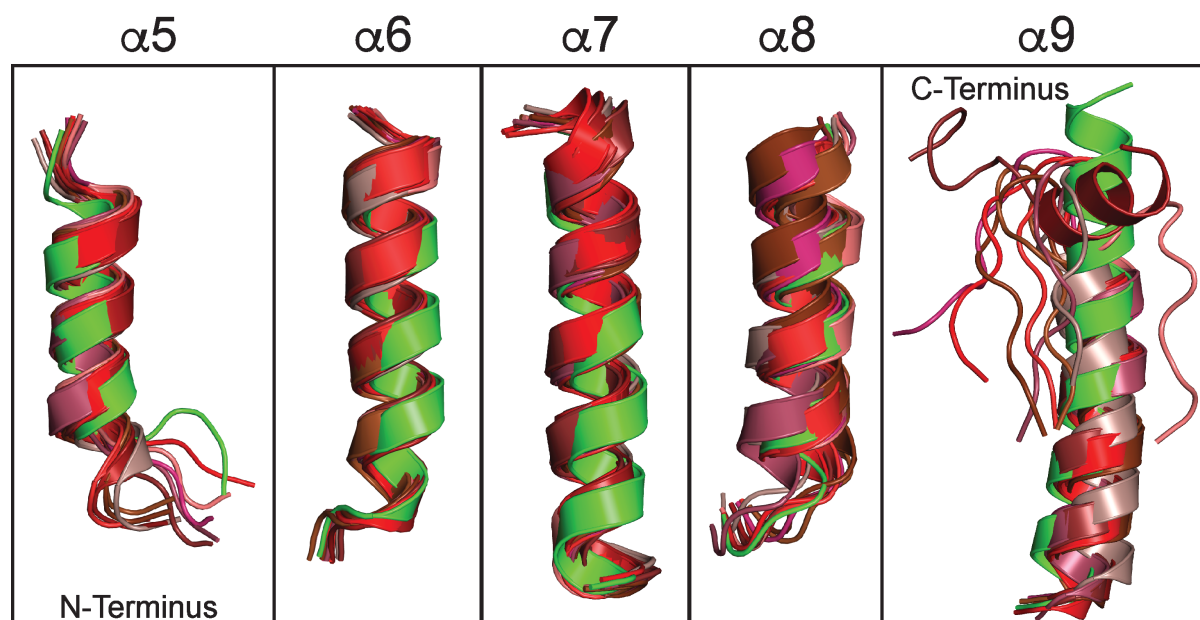


Figure S6. Comparison of the individual α -helices of the Top10 conformers (plotted in shades of red) with the first conformer of 2M66 (green) following global superimposition of the structures. Helices 5-7 align more closely than helices 8 and 9.

References

- (1) Yagi, H., Pilla, K. B., Maleckis, A., Graham, B., Huber, T., and Otting, G. (2013) Three-dimensional protein fold determination from backbone amide pseudocontact shifts generated by lanthanide tags at multiple sites. *Structure* 21, 883–890.
- (2) Schmitz, C., Stanton-Cook, M. J., Su, X.-C., Otting, G., and Huber, T. (2008) Numbat: an interactive software tool for fitting $\Delta\chi$ -tensors to molecular coordinates using pseudocontact shifts. *J. Biomol. NMR* 41, 179–189.
- (3) Stanton-Cook, M. J., Su, X.-C., Otting, G., and Huber, T. (2010) PyParaTools. <http://comp-bio.anu.edu.au/mscook/PPT/>, accessed April 25, 2019.
- (4) Barak, N. N., Neumann, P., Sevvana, M., Schutkowski, M., Naumann, K., Malešević, M., Reichardt, H., Fischer, G., Stubbs, M. T., and Ferrari, D. M. (2009) Crystal structure and functional analysis of the protein disulfide isomerase-related protein ERp29. *J. Mol. Biol.* 385, 1630–1642.
- (5) The PyMOL Molecular Graphics system, Version 2.0 Schrödinger, LLC.